Analytical 4D Infrared Tomography Using an InSb Focal Plane Array Sensor. 2. 4D Infrared Tomography (Multiwavelength Approach)

ARTICLE *in* ANALYTICAL CHEMISTRY · NOVEMBER 1996

Impact Factor: 5.64 · DOI: 10.1021/ac960121a

2 AUTHORS, INCLUDING:

Karl Cammann
University of Münster
365 PUBLICATIONS **3,615** CITATIONS

Anal. Chem. **1996,** *68,* 3994−3999

Analytical 4D Infrared Tomography Using an InSb Focal Plane Array Sensor. 2. 4D Infrared Tomography (Multiwavelength Approach)

D. Wienke*,† and K. Cammann‡

SONY Germany GmbH, Stuttgart Technology Centre, Environmental Centre Europe, Stuttgarter Strasse 106, D-70736 Stuttgart-Fellbach, Germany, and Institute for Analytical Chemistry, Wilhelms-University of Münster, Mendel-Strasse 8, 48149 Münster, Germany

A focal plane array InSb image detector has been used for noninvasive spectroscopic infrared tomography of visually turbid polymer bodies. Tomographic images from a rotating sample, illuminated by infrared light, were taken under distinct, equidistant angular views. Several IR wavelengths were used simultaneously for illumination. This provided for each analyzed sample a four-dimensional data set consisting of three geometric dimensions (x, y, z) and the wavelength axis (λ). Concealed or secret parts inside the turbid hollow polymer body were visualized by three-dimensional numerical computer-assisted tomographic reconstruction using the back-projection algorithm. IR tomography at different wavelengths provided the possibility of differentiation between distinctly absorbing materials inside a visually turbid material. The name 4D IR tomography or spectroscopic infrared tomography is proposed for this new analytical method.

The preceding paper[1] described the experimental use of a focal plane InSb detector array (FPA) for "tomographic imaging" of visually turbid polymer samples. Distinctive absorbing hidden objects such as liquids or metals became visual inside nontransparent polymer bodies. A series of angular views from such a polymer body provided a full three-dimensional computer-reconstructed view of hidden parts. This approach is comparable, for example, to computer-assisted X-ray tomography in medicine applied to the analysis of the human body. However, the use of near-IR and mid-IR radiation in place of X-rays is chemically and analytically more interesting for polymer and drug analysis or for the analysis of liquids and turbid emulsions, for example. The present work extends the former study from 3D infrared tomography (single-wavelength approach) to 4D infrared tomography (multiwavelength approach). The new analytical technique is called tomography or "spectroscopic infrared tomography" (SIT). From the point of view of IR spectroscopy (respectively near-IR spectroscopy) as a spatially one-dimensional working method and from the point of view of IR imaging spectroscopy as a spatially two-dimensional working technique,[2−12] SIT has to be considered as a generalization to the third spatial dimension.

This evolutionary hierarchical relation between infrared spectroscopy, infrared spectroscopic imaging and spectroscopic IR tomography was explained recently in Figure 1 of ref 1. SIT samples an object in its three spatial dimensions simultaneously and additionally at several infrared wavelengths. This high-end approach provides not a three-dimensional but a four-dimensional data set for each analyzed sample.

Infrared tomography is generally classified in the group of optical tomography methods. In refs 1, 15, and 33, the state-of-

† SONY.

‡ Wilhelms-University of Münster.

(1) Wienke, D.; Cammann, K. *Anal. Chem.* **1996**, *68*, 3987−3993.
(2) Lewis, E. N.; Levin, I. A. *Appl. Spectrosc.* **1995**, *49* (5), 673−678.
(3) Treado, P. J.; Levin, I. W.; Levis, E. N. *Appl. Spectrosc.* **1994**, *48* (5), 607−615.
(4) Robert, P.; Bertrand, D.; Devaux, M. F. *NIR News* **1991**, *2* (2), 9−10.
(5) McClure, W. F. *NIR News* **1991**, *2* (2), 8.
(6) Geladi, P.; Grahn, H.; Lindgren, F. In *Applied Multivariate Analysis in SAR and Environmental Studies*; Devillers, J., Karcher, W., Eds.; Kluwer Scientific Publishers: Amsterdam, 1991; pp 447−478.
(7) Lewis, E. N.; Treado, P. J.; Reeder, R. C.; Story, G. M.; Dowrey, A. E.; Marcott, C.; Levin, I. W. *Anal. Chem.* **1995**, *67*, 3377−3381.
(8) Wienke, D.; v. d. Broek, W.; Melssen, W.; Buydens, L. *Proceedings, INCOM'95* (Instrumentalized Analytical Chemistry and Computer Technology Conference); Dusseldorf, Germany, March 1995; p 479.
(9) v. d. Broek, W.; Wienke, D.; Melssen, W.; Buydens, L. *Proceedings of the NIR-95 Conference, The Future Waves*, 7th International Conference on Near-Infrared Spectroscopy, Montreal, Canada, 6−11 August 1995; p 42.
(10) v. d. Broek, W.; Wienke, D.; de Crom, K.; Melssen, W.; Buydens, L. *Anal. Chem.* **1995**, *67*, 3753−3759.
(11) Wienke, D.; v. d. Broek, W.; Buydens, L. *Anal. Chem.* **1995**, *67*, 3760−3766.
(12) Wienke, D.; van den Broek, W.; Huth-Fehre, T.; Kantimm, T.; Feldhoff, R.; Winter, F.; Cammann, K.; Buydens, L. *Fresenius J. Anal. Chem.* **1996**, *354*, 823−826.
(13) Ewing, J. *Neoplastic Disease*; Saunders: Philadelphia, PA, 1928.
(14) Cutler, M. *J. Surg. Gyneacol. Obstet.* **1929**, *48*, 721−728.
(15) Profio, A. E.; Navarro, G. A.; Sartorius, O. W. *Med. Phys.* **1989**, *16*, 60−65.
(16) Herman, G. T. *Image Reconstruction from Projections*; Academic Press: New York, 1980.
(17) Singer, J. R.; Grünbaum, F. A.; Kohn, P.; Zubelli, J. P. *Science* **1990**, *248*, 990−993.
(18) Verhoeven, D. *Appl. Opt.* **1993**, *32*, 3736−3754.
(19) Wison, B. C.; Sevick, E. M.; Patterson, M. S.; Chance, B. *Proc. IEEE* **1992**, *80* (6), 918−930.
(20) Sevick, E. M.; Lakowicz, J. R.; Scmacinski, H.; Nowaczyk, K.; Johnson, M. L. *J. Photochem. Photobiol., B: Biol.* **1992**, *16*, 169−185.
(21) Arridge, S. R.; Schweiger, M.; Hiraoka, M.; Delpy, D. T. *Proc. SPIE-Int. Soc. Opt. Eng.* **1992**, *1888*, 360-371.
(22) Gratton, E.; Mantulin, W. W.; van de Ven, M.; Fishkin, B. J.; Maris, M. B.; Chance, B. *Bioimaging* **1993**, *1*, 40−46.
(23) Chance, B.; Kong, K.; Sevick, E. *Opt. Photonics* **1993**, *10*, 9−11.
(24) Benaron, D. A.; Stevenson, D. K. *Science* **1993**, *259*, 1463−1466.
(25) Kalpaxis, L. L.; Wang, L. M.; Galland, P.; Liang, X.; Ho, P. P.; Alfano, R. R. *Opt. Lett.* **1993**, *18*, 1691−1693.
(26) Das, B. B.; Yoo, K. M.; Alfano, R. R. *Opt. Lett.* **1993**, *18*, 1092−1094.
(27) Anderson, G. E.; Liu, F.; Alfano, R. R. *Opt. Lett.* **1994**, *19*, 981−994.
(28) Benaron, D. A. *Laser Focus World* **1994**, *1*, 79−87.
(29) Dolne, J. J.; Yoo, K. M.; Alfano, R. R. *Lasers Life Sci.* **1994**, *6*, 131−141.
(30) Sevick-Muraca, M. E.; Burch, C. L. *Opt. Lett.* **1994**, *23*, 1928−1930.
(31) Alfano, R. R.; Liang, X.; Wang, L.; Ho, P. P. *Science* **1994**, *264*, 1913−1914.
(32) Sevick, E. M.; Frisoli, J. K.; Burch, C. L.; Lakowicz, J. R. *Appl. Opt.* **1994**, *33*, 3562−3570.

S0003-2700(96)00121-7 CCC: $12.00

the-art of optical tomography (note: non-X-radiation) and its history[13,14] within medicine has been discussed. Alfano and co-workers,[25−27,29,31] Benaron's medical physics laboratory,[24,28] and the research groups of Sevick-Muraca[20,30,32] and Chance[19,22,23] developed elegant techniques for looking through optically turbid media. These four laboratories especially deal with the medically interesting optical window between 600 (visible light) and 1300 nm (short-wave near-IR). Radiation of this wavelength range easily passes into the human body for distances of several centimeters up to decimeters, providing shadow images for a tomographic reconstruction of hidden body parts. A related technique, called "near-infrared topography" for medicine combines several single detectors located at a patients head as a network.[36−38] Other recent studies published new mathematical reconstruction algorithms for optical tomograms.[16−18]

Only a few applications for optical tomography were reported in the chemical literature. Otoki, Kuma and co-workers[34,35] mentioned its potential for quality control of semiconductor materials based on thermal emission but without describing any tomographic detail. Monnig et al.[39,40] studied the three-dimensional distribution of several emission parameters within an ICP plasma in the optical UV/visible range. Todd and Ramachandran[41,42] combined an FT-IR spectrometer having a spatially moveable beam with many single infrared mirrors which were mounted on a room's walls. In this way, the authors were able to get the tomographically reconstructed indoor air 3D pollution profile.

The present work also focuses on the chemically and analytically interesting optical window of the higher near-infrared to the mid-infrared optical region (1100−5000 nm) but makes use of the new FPA technology in place of a classical spectrometer. Within this optical window a lot of chemically important materials show characteristic and distinct absorption bands for future tomographic discrimination.

Chemists were always interested in noninvasive analytical methods for the study of three-dimensional samples. It is still a fascinating dream for many analytical chemists and spectroscopists to visualize hidden chemical objects inside a nontransparent sample in a noninvasive and remote way. Visually turbid specimen such as polymers, glasses, drugs, emulsions, powders, or opaque liquids are of particular analytical and technical interest for future study by SIT. The present work continues to explore the fundamental principle of IR tomography for analytical chemistry. Modern infrared FPA technology is combined with enhanced computer power and mathematical algorithms for tomographic

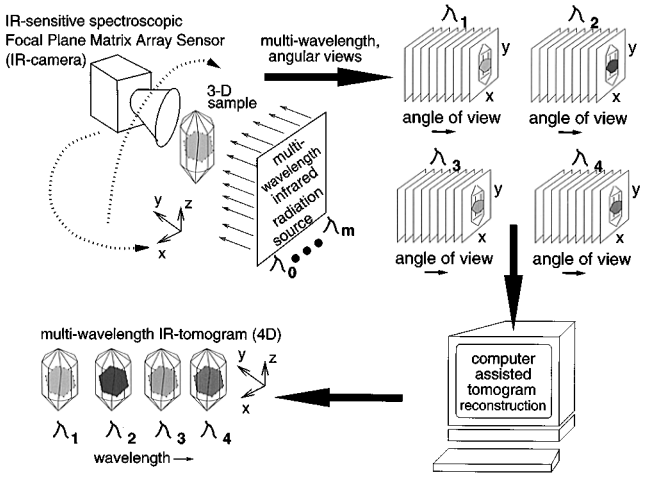

Figure 1. Four-dimensional infrared tomograms from a three-dimensional sample obtained by observation under distinct angular views and simultaneously at different wavelengths. The required distinct angular views are provided by a relative mutual rotation of the sample to the focal plane array sensor. The necessary wavelength selection is reached by a spectrometric part (here not drawn) in the optical path between infrared radiation source and focal plane array sensor such as interference filters, AOTF filters, or an interferometer.

4D image reconstruction. Again different model systems consisting of turbid material of a few millimeters thickness including hidden samples were applied for this fundamental study.

3D , 4D, AND 5D INFRARED TOMOGRAPHY

The difference between 4D and 3D optical tomography is the simultaneous use of more than one wavelength or a full spectrum instead of a single wavelength only (or wavelength range) (Figure 1). The three-dimensional sample is pointless when analyzed in the geometric *x*, *y*, *z* space and simultaneously at distinct observation wavelengths (or by measuring a full spectrum) for each spatial point. This results in a four-dimensional data set for a single three-dimensional sample (the four dimensions are *x y z* wavelengths). Therefore, for each single observation wavelength λ_i, a three-dimensional stack of infrared images is obtained (Figure 1, right upper corner). According to the absorbency of the distinct hidden materials for each specific wavelength, this will result in distinct gray level ratios for these materials within each individual image stack. This has been symbolized in Figure 1 by the four distinct gray value levels in the four image stacks (right upper corner). By means of a powerful computer, the 3D tomogram can be reconstructed for each single wavelength, providing in total the so-called multiwavelength or 4D infrared tomogram (Figure 1, lower left corner). Note, that less or more than four wavelengths can be chosen. (The arbitrary number of four wavelengths chosen in the example of Figure 1 is not related to the expression "4D"). The choice of suitable optical wavelengths provides some additional opportunities for quantitative infrared tomographic analysis. At some wavelengths, selected hidden materials will become transparent and will not disturb the visibility of other hidden materials which just absorb at this wavelengths. This 4D tomographic approach enables the visualization of distinctively absorbing objects inside a 3D sample by tuning the spectral observation wavelength.

There seems to be another important advantage of the 4D technique over 3D tomography. 4D infrared tomograms form

(33) Leutwyler, K. *Sci. Am.* **1994**, *1*, 130−131.
(34) Otoki, Y.; Watanabe, M.; Inada, T.; Kuma, S. *J. Cryst. Growth* **1990**, *103*, 85−90.
(35) Kuma, S.; Otoki, Y. *Institute of Physics Conference Series 135*; IOP Publishing Ltd.: London, 1994; Chapter 4, pp 117−126.
(36) Maki, A.; Yamashita, Y.; Ito, Y.; Watanabe, E.; Mayanagi, Y.; Koizumi, H. *Med. Phys.* **1995**, *22* (12), 1997−2005.
(37) Watanabe, E.; Yamashita, Y.; Maki, A.; Ito, Y.; Koizumi, H. *Neurosci. Lett.* **1996**, *205*, 41−44.
(38) Yamashita, Y.; Maki, A.; Koizumi, H. *Rev. Sci. Instrum.* **1996**, *67* (3), 730−732.
(39) Monnig, C. A.; Marshall, K. A.; Rayson, G. D.; Hieftje, G. M.; *Spectrochim. Acta* **1988**, *43B* (9−11), 1217−1233.
(40) Monnig, C. A.; Gebhardt, B. D.; Marshall, K. A.; Hieftje, G. M. *Spectrochim. Acta* **1990**, *45B* (3), 261−270.
(41) Todd, L.; Ramachandran, G. *Am. Ind. Hyg. Assoc. J.* **1994**, *55* (5), 403−417.
(42) Todd, L.; Ramachandran, G. *Am. Ind. Hyg. Assoc. J.* **1994**, *55* (12), 1133−1143.

generalized data matrices or so-called tensors which could be treated by principal component analysis, for example, to extract "hidden data structures". From his chemometrical perspective and his experience in data analysis of multiwavelength images[10−12] the author intuitively feels that this 4D approach could provide in future some new opportunities for multivariate analysis of this type of data. This will only be mentioned here but will be evaluated in a up-coming 4D infrared tomographic study in more detail.

Theoretically, one could imagine that time-dependent chemical processes could also be observed by SIT, such as the dynamic three-dimensional distribution of reactants in a reaction vessel. Another example could be an observation of the spatially resolved, time-dependent change of properties of a solid polymer/copolymer. The variable "time" adds an axis to the data space, providing a further generalization called 5D tomography or "spatiotemporal infrared spectroscopic tomography".

The present study concentrates on the experimental aspect of 4D tomography with an InSb FPA sensor.

EXPERIMENTAL SECTION

Experimental Setup. The main details of the setup for spectroscopic IR tomography were given in Figure 2 of the preceding paper.[1] An axial rotating sample is placed in the optical path between a broad-band infrared illumination source and an InSb FPA camera IRC-64 (Cincinnati Electronics Inc., Cincinnati, OH). This optically turbid sample, during its horizontal rotation around its vertical axis, presents a series of distinct angular views to the FPA detector. Strong infrared radiation passes the turbid sample in transmission mode. Hidden objects inside the turbid sample provide shadow projections onto the outer sample surface. These shadow projections form the data basis for a numerical, computer-assisted tomographic reconstruction technique. For each angle of view, the FPA detects an infrared shadow image, a reference image, and a dark current image for spectral image baseline correction. Optical infrared filters between FPA and the sample allow one to view at distinct wavelengths simultaneously ("spectroscopic tomography"). It is obvious that SIT enables the analysis of turbid samples that have only a few millimeters thickness due to the significant high absorption coefficients for mid-IR and near-IR radiation and due to the scattering characteristics of the analyzed turbid material. The camera is connected via a digital interface to a workstation. The workstation records the images for each angle of view and for the selected distinct optical wavelengths. One completed tomographic sample measurement provides a four-dimensional data set of $n \times m \times w \times v$ absorption values. $n \times m$ is the detector array size of the FPA camera (here, 64×64) or simply the image dimension. v is the number of horizontal angular viewing steps of the rotating sample. In the present setup, 64 discrete steps can be realized, which corresponds to a minimum rotation angle step width of $360/64 = 5.625°$. w is the number of spectroscopic infrared wavelengths that are simultaneously scanned for each viewing angle over the IR spectral region. In the present study, $w = 6$ wavelengths were used to study tomographic model material systems. Wavelengths are automatically chosen by a rotating filter wheel.

Software and Computations. Recorded images from different viewing angles were saved on hard disk as matrices in flat ASCII code and further processed by the back-projection algorithm[16] implemented by the author in MATLAB code.

Materials and Methods. The infrared tomographic model material system consisted of tubes of distinct turbid materials [sanded quartz glass, white milky poly(tetraflourethylene) (PETF) and white milky poly(oxymethylene) (POM)]. Tube length was 100.0 mm, outer diameter was 40.0 mm, and the wall thickness was 1.0, 2.0, or 4.0 mm. For the three chosen tube materials their wall thickness was already enough to make them nontransparent for the human eye. Note, that the IR radiation penetrated both walls of each tube in transmission to reach the FPA sensor. Several specimens were placed inside each visual nontransparent turbid tube. These "hidden specimens" were made from materials with absorption coefficients different from the tube material such as pieces of polystyrene, polypropene, and calcium silicate glass. The experimental aim was to "find" these "hidden specimens" by IR radiation and to reconstruct their position, shape, and size in a computer-calculated tomographic 3D space for each given IR wavelength. In an initial experiment, several tube materials with several hidden objects were combined and visualized under only one angle of view without tomographic rotation. For this experiment, mid-infrared and near-infrared radiation was used. For the tomographic 4D reconstruction experiment, 16 viewing angles were chosen to get an acceptable computer-calculated 3D image of the hidden specimens. The tube was observed at six different near-infrared wavelengths simultaneously. The reconstructed 3D image for each of the wavelengths is built from a vertical stack of 64 calculated, horizontal tomographic slices of individual size of 91×91 pixels. The height of 64 slices for such a calculated vertical 3D stack is derived from the vertical observation height of 64 pixels of the InSb FPA sensor. The squared dimension of 91×91 pixels per individual calculated tomographic slice originates from the circular superposition of the 16 original images with a width of 64 pixels. This width is directly related to the horizontal observation width of the FPA of 64 pixels. Examples for this are given in Figure 7 of the preceding paper.[1] The maximum geometric extension of 91×91 calculated pixels originates from the domination of the image diagonal of length $d = (64^2 + 64^2) = 90.51$ during the back-projection procedure, which has been finally rounded to 91 full pixels. The computer-assisted back-projection of the 16 infrared images (each of resolution 64×64 pixels) onto all $91 \times 91 \times 64 = 529\,984$ voxels ("volume pixels") required a significant calculation time on a SUN Spark 10 computer workstation (stand alone) with 32 Mbytes of RAM memory. For a single slice, total 128 s of computation time was needed. To get the fully reconstructed 3D infrared tomogram for a single turbid sample took in total 64×128 s $= 8192$ s (more than 2 h of CPU time). The 3D reconstruction had to be done for each chosen wavelength separately. The 4D reconstruction (six 3D tomograms at six wavelengths) required around 13 h of CPU time.

RESULTS AND DISCUSSION

Figure 2 and Figure 3 give a first impression about the absorption of distinct materials, hidden inside of turbid tubes. From Figure 2 one can see that PTFE and quartz are more transparent than the polymer material POM. In particular, the view through the Teflon tube is exciting. One can clearly recognize the rectangular shape of a hidden piece of polystyrene. The sample has a thickness of 2 mm. Nevertheless the paper sticker, which is located at the back side of the PS slice from the point of view of the FPA sensor, is also visible. In other words,

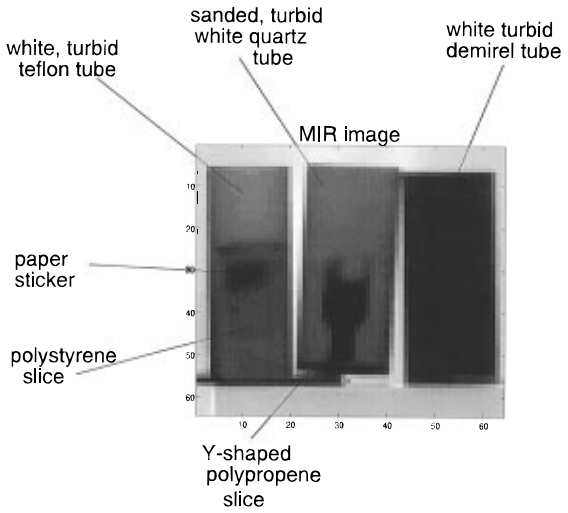

Figure 2. Three turbid tubes of identical outer diameter (40.0 mm) and identical wall thickness (1.0 mm), but distinctively absorbing materials observed in the optical mid-infrared window between 2.3 and 4.6 μm with a InSb focal plane array sensor. More bride gray levels correspond to less absorption (higher transmission). The quartz tube and the Teflon tube are partially transparent in this optical window, and they allow the visualization of inside hidden objects. Note that the paper sticker is located at the back side of the piece of polystyrene, which means that the FPA has to look through two Teflon and through one polystyrene layer in succession.

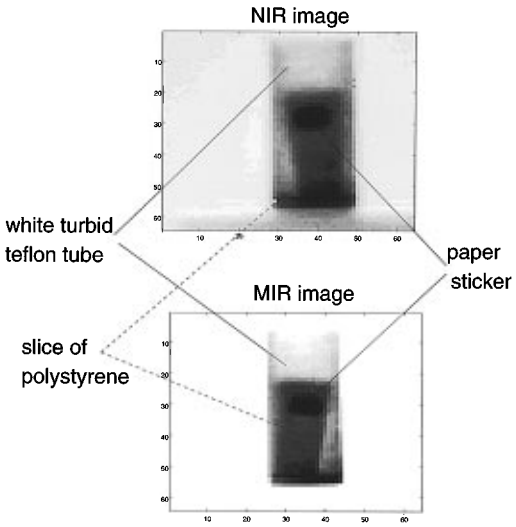

Figure 3. Comparison of the broad-band mid-IR and near-IR images taken in the wide-range optical ranges from 2.3 to 4.6 μm (respectively from 1.1 to 2.6 μm). More bride gray levels correspond to less absorption (higher transmission). Note that the paper sticker is placed at the back of the piece of polystyrene, so that the FPA sensor has to look through the wall of two Teflon tubes as well as through the polystyrene slice.

the FPA sensor "looks through" the wall of the PTFE tube and through the white turbid PS slice. Figure 3 proves that such a transparent view through three different material layers is possible in the mid-infrared as well as in the near-infrared region. Note, that the InSb FPA sensor is sensitive to radiation between 1.1 and 4.5 μm, which makes it suitable for near-IR and for mid-IR measurements. Note further that, for both initial experiments (near-IR, mid-IR) in Figures 2 and 3, no specific wavelength was chosen but the full near-IR (respectively mid-IR) optical wavelength range was used. To realize these experiments, in the case of the near-IR image, a boron crown glass camera lens (BK7)

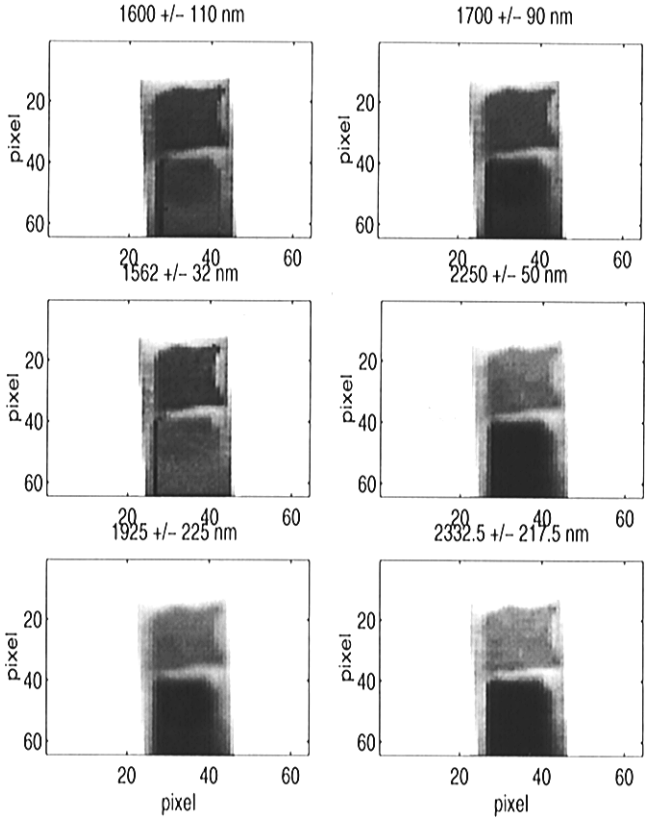

Figure 4. Near-IR tomographic multiwavelength image of the same axial-rotated Teflon tube as used in Figure 4 under the tomographic observation angle of 0.0° but simultaneously taken at six distinct near-IR absorption wavelengths. A glass slice (above) and polymer slice (below) were hidden inside the white turbid Teflon tube. Dark pixel gray levels correspond to stronger near-IR absorption. Note the inverse absorption of both hidden material slices at 1562 and at 2250 nm (second row of images, Figure 7). The same holds for the two images at 1600 and 1700 nm (first row).

served simultaneously as broad-band filter. It only enabled near-IR radiation to pass the lenses. In the other case of mid-IR imaging, the thermography lens of the FPA camera served as a broad-band filter to exclude the near-IR radiation from the analysis. A new cold shield blocked the background radiation above 4.5 μm.

Figure 4 demonstrates the first result from a multiwavelength infrared tomographic experiment with the FPA sensor. The differences in absorbency of a piece of calcium silicate glass and a piece of polystyrene inside the turbid Teflon tube are visible (see also Figure 7). The 4D tomographic experiment was fully completed by a rotation of the tube at each of those wavelengths under 16 angular views, as given, for example, in Figure 5. From the 16 angular views of the tube, its hidden inner parts have been reconstructed by the back-projection algorithm (Figure 6). The back-projection algorithm is a spatial superposition of all 16 angular views, providing for each wavelength the 3D tomogram. This superposition comes down to a summation of gray value intensities at each voxel location in the 3D space. In this way, the infrared absorbency ratios are conserved from the measured images (Figures 4 and 5) throughout the computer reconstruction of the tomograms in Figure 6.

Toward Quantitative Analytical 4D Tomography. It is fascinating and exciting for each spectroscopist to have an opportunity for visualization of an hidden absorber inside a visually turbid medium (here, Teflon tube). For medical applications, this

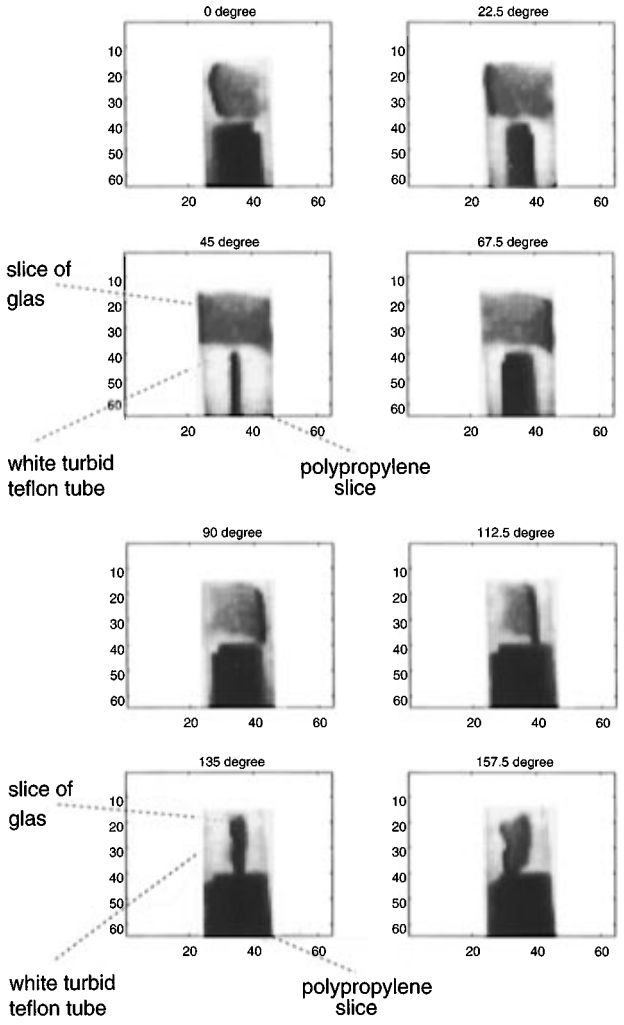

Figure 5. Eight near-infrared images of a rotating Teflon tube of 40.0 mm diameter and 2.0 mm wall thickness taken under eight tomographic axial angular views with the InSb FPA sensor. Bride gray levels correspond to less absorption (higher transmission, Figure 7). The selected near-IR wavelength window was from 2115 to 2550 nm. (compare to Figure 4, bottom right). A slice of brown glass (top) was fixed (from a beer bottle) inside the white, turbid Teflon tube. Below the glass slice, a slice of white turbid polypropene (2.0 mm thick) was fixed at an angle of 90° relative to the position of the glass.

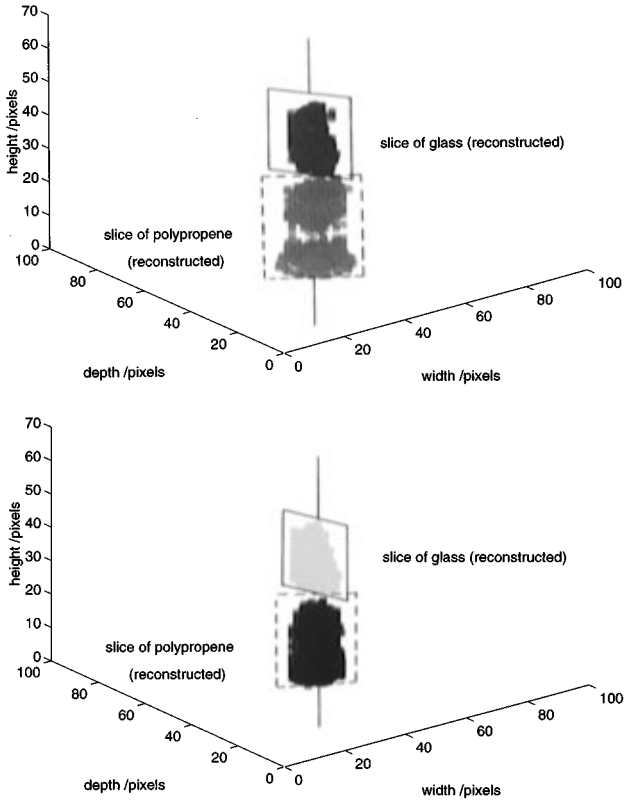

Figure 6. Computer-reconstructed 4D infrared tomograms of the hidden material slices inside the white turbid Teflon tube (from Figures 4 and 5) for two near-IR wavelength ranges (1562 nm, top) and (2250 nm, bottom). Gray value levels correspond to the distinct measured absorptions of the glass slice and of the polypropene slice at these wavelengths (Figure 7). For simplicity, the Teflon tube has been removed but its vertical central axis is indicated by a thick line. For visual convenience, the spatial location planes for the glass slice (solid rectangular) and for the polypropene slice (dashed rectangular) are indicated.

qualitative tomography already means a lot. But an analytical chemists more accepting of a new method such as 4D infrared tomography if it also will enable him to perform a quantitative analysis. Looking for more quantitative 4D tomography, three opportunities seem to be interesting: (1) 3D shape and 3D size analysis of hidden objects; (2) determination of the object location in the 3D space; and (3) determination of spatial analyte concentrations and spatial analyte distributions.

Items (1) and (2) were demonstrated in Figures 4−6. The third possibility directly follows (1) and (2). If the thickness and the absorbency of a hidden object was reconstructed by a tomogram such as shown in Figure 6 for a given wavelength, the concentration should become directly analyzable via Lambert−Beer's law. It should be mentioned that the thickness of tomographic objects such as the slices of glass and polymer in Figure 6 can be determined in the computer at each spatial sample position, in principle. Such computer-stored tomographic objects are quite comfortable to rotate, to handle, and to characterize. The added value of further wavelengths in 4D tomograms is that one can construct a system of linear equations for multicomponent determinations. It is obvious that all spectroscopic information that is present in an infrared spectrum (respectively in a multivariate infrared image) is also contained in a 4D tomogram. This should allow the analytical chemist quantitative studies via 4D infrared tomograms with their added value of pointless spatial sample resolution.

CONCLUSIONS

Future analytical research will show far the proposed method of 4D infrared tomography with FPA sensor can be applied to the spatial determination of hidden objects and analyzes inside of turbid analytical samples. In the present work, the fundamental possibilities of the new focal plane array sensor technology for the purpose of analytical 4D IR tomography has been introduced. With such a new FPA detector, originating from thermographic detection systems in high-tech weapons (missiles, rockets, tanks), the analytical chemist gets a fascinating research instrument in his hands. Several applications have to be considered in the future for this new method. One can think about the spatial IR tomographic distribution analysis of active compounds in pharmaceutical products or in technical emulsions. Further applications could be the spatial homogeneity analysis of polymers, rubbers, ceramics, or glasses (if their absorbency properties and

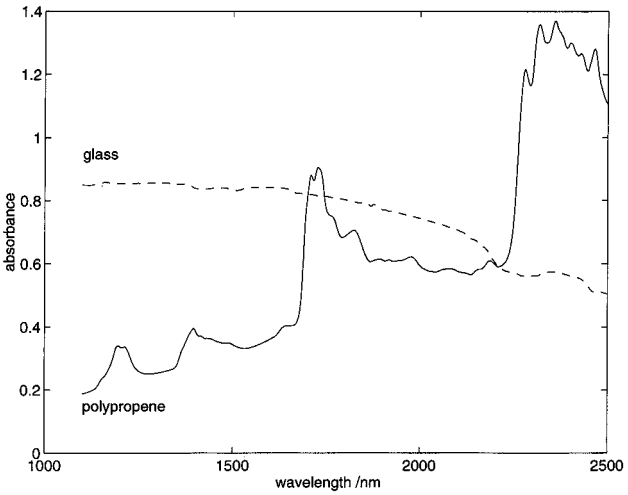

Figure 7. Near-IR spectra of the slice of glass (dashed line) and polypropene used in the tomographic experiments (Figures 4−6). Note that the relative absorption ratios for both materials are inverse for the two optical regions above 2200 nm and below 2200 nm (comparable sample thickness assumed). This finds its quantitative expression in distinct gray level ratios in the tomographic multiwavelength image in Figure 5 and finally in the calculated 4D infrared tomogram (Figure 6).

their sample size are suitable enough). New FPA sensors recently became available with pixel resolutions of 256 × 256 and still more and with an acquisition rate of up to 1000 images/s. In combination with rapid imaging spectrometers and computers, one can imagine that under these circumstances an analytical tomogram of a piece of sample will take only a few seconds or milliseconds. Furthermore, one can also speculate about a rapid IR tomographic monitoring of volume reactions ("5D tomographic kinetics") and IR tomographic process control. But before this can become true, improvements in detector resolution, sample excitation, optics, and tomographic data processing have to be applied to the experiments demonstrated in the present work to get a reliable and routine analytical method.

ACKNOWLEDGMENT

The authors are grateful to Prof. Heinz Siesler and Prof. Bernhard Schrader (both at the University of Essen, Essen, Germany) for their independent comments about the manuscript before its submission. Thanks to the Laboratory of Analytical Chemistry (University of Nijmegen, The Netherlands) for technical assistance and to the European Commission for financial support. Dedicated to the 100th anniversary of Conrad Roentgen's discovery of X-rays—1895−1995.

Received for review February 6, 1996. Accepted August 3, 1996.[⊗]

AC960121A

[⊗] Abstract published in *Advance ACS Abstracts,* September 15, 1996.